All-Optical Fiber Photoacoustic Gas Sensor with Double Resonant Enhancement

Congzhe Zhang, Yuanhong Yang, Yanzhen Tan, Hoi Lut Ho, and Wei Jin, *Senior Member, IEEE*

Abstract—An all-optical fiber photoacoustic gas sensor with double resonant signal enhancement is presented. The sensor uses a fiber-tip graphene nano-mechanical resonator operating at one of its resonances as the acoustic detector and a micro-acoustic resonant tube, whose resonant frequency is matched to that of the graphene resonator, as the PA gas cell. Compared with the single resonant detection with a graphene resonator, a five-fold signal enhancement is achieved. With 138 mW pump power and 1 second lock-in time constant, a noise equivalent concentration of ~25 ppb C_2H_2 is achieved, corresponding to a normalized noise equivalent absorption of $1.29x10^{-8}$ $cm^{-1}WHz^{-1/2}$.

Keywords: Gas detectors, photoacoustic spectroscopy, optical fiber sensors, acoustic resonators.

I. Introduction

Photoacoustic spectroscopy (PAS) has been extensively studied for trace gas detection and demonstrated high sensitivity and selectivity [1]. This technique converts periodic light absorption of gas molecules into acoustic pressure wave via the photoacoustic (PA) effect and obtains the gas concentration by detecting the acoustic signal. With advanced laser sources and acoustic detectors in combination with optimized modulation methods, PAS gas sensors have demonstrated sub-parts per billion (ppb) level detection limit [2-4]. However, most of the PAS systems reported so far used electrical microphones such as condenser microphones and quartz tuning forks, which have limitations for applications in harsh environments and for remote detection.

Attempts were made to develop optical and fiber-optic microphones for PA signal detection. Cantilever enhanced PA detection was reported by K. Wilcken et al [5, 6]. In combination with an optical Michelson interferometer, very high sensitivity gas detection has been achieved [6]. However, this setup is complex and uses free-space optics, which are unsuitable for long-distance signal transmission. Diaphragm-based optical fiber-tip Fabry-Pérot interferometer (FPI) sensors were studied for pressure/acoustic detection and applied to PA gas sensors [7, 8]. Wang et al reported gas detection down to ppb level with a longitudinal resonant PA cell of 10-cm in length and 1-cm in diameter. They used an excitation optical power level of ~0.5 Watt, a gold-coated reflecting mirror to increase the gas absorption length, and a polymer diaphragm-based fiber-tip FPI for acoustic detection [9]. A miniature fiber-tip gas sensor which used a FPI cavity as the acoustic detector as well as the gas cell was reported [10]. This configuration reduced the dimension of sensor down to ~mm scale but still achieved a lower detection limit of 4.3 ppm C_2H_2 with excitation power of 8 mW. The sensitivity of the FPI sensor is greatly affected by the dimension of the diaphragm. To achieve higher sensitivity, thinner diaphragm with a larger diameter is needed [11]. Recently, we reported an all-optical fiber PA gas sensor by use of a 100-nm-thick graphene nano-mechanical resonator as the acoustic detector [12]. With a non-resonant PA cell, the system achieved a lower detection limit of ~120 ppb with ~124 mW pump power.

In this letter, we report a novel double-resonant signal enhancement technique to achieve higher sensitivity gas detection with a compact PA cell. We employ a graphene nano-mechanical resonator operating at one of its mechanical resonances as the acoustic detector and a miniature acoustic resonant tube of 4.3-mm-long and 1-mm in diameter as the resonant PA cell. The design of the PA cell is optimized so that its resonant frequency matches to that of the graphene nano-mechanical resonator to achieve double PA signal enhancement.

II. Experimental Setup

A schematic diagram of the experimental system is shown in Fig. 1. Wavelength modulation spectroscopy with second harmonic (2*f*) detection method was employed for measuring the PA signal. A distributed feedback (DFB) laser (Furukawa Electric Co. Ltd, FLD5F15CX805W9560L) with an emission wavelength around 1532 nm is used as the pump source for PA excitation. Its wavelength is modulated sinusoidally by use of the internal signal generator of a lock-in amplifier (LIA) (Stanford Research Systems, SR830) and simultaneously swept slowly across the P(13) absorption line of acetylene (C_2H_2) at 1532.83 nm by using a function generator (Stanford Research Systems, DS345). The P(13) line is in the v_1+v_3 band and has a line strength of 1.035^{-20} $cm^{-1}/molec \cdot cm^{-2}$. An optical fiber amplifier (OFA) is used to amplify the pump light to achieve a higher power level. A tunable filter is placed after the OFA to reduce the amplified spontaneous emission (ASE) noise. The amplified pump light is collimated to a beam diameter of ~300 μm and injected into an acoustic resonant tube, which acts as the resonant gas cell. The acoustic detector is a multi-layer graphene diaphragm-based FPI microphone that has ultra-high acoustic sensitivity [7]. An external-cavity diode laser (ECDL) (Agilent, 81600B) is used as the probe light source for the microphone. The probe light is delivered to the acoustic detector via an optical circulator (OC) and partially reflected by the FPI. The reflected light is converted to electrical signal by a photo-detector (PD). The electrical signal is demodulated by the LIA at its 2*f*-frequency and recorded by a data acquisition (DAQ) card for post-processing.

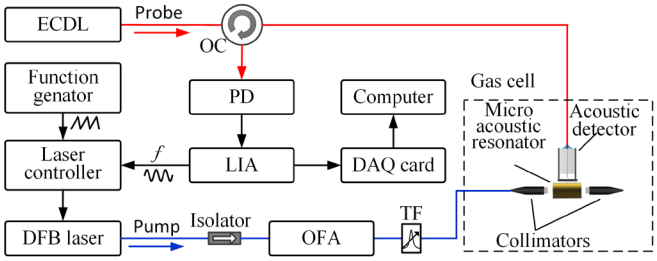

Fig. 1 Schematic of the experimental setup. Red line, Probe light path, Blue line, Pump light path, Black line, electrical signal path; ECDL, external-cavity diode laser; PD, photo-detector; OFA, optical fiber amplifier; LIA, lock-in amplifier; DAQ, data acquisition; DFB laser, distributed feedback laser; TF, tunable filter.

The configuration and photograph of the fiber-tip microphone is shown in Fig. 2, which is similar to that described in [13]. A multi-layer graphene diaphragm with thickness of ~100 nm is attached at the end of a ceramic sleeve by ultraviolet curable adhesive. The effective diameter of graphene membrane is determined by the sleeve inner diameter and is ~2.5 mm. A ferrule containing a cleaved single mode fiber (SMF) is inserted from the other end of the sleeve. The junctions of components are glued with epoxy adhesive to keep the configuration firm. A low-finesse FPI is then formed between the endface of the fiber and the surface of the graphene diaphragm. Probe light injected into the fiber is partially reflected by the fiber endface and the surface of diaphragm that has a reflectivity of ~2.5%. Due to the low reflectivity of the two surfaces, higher-order light reflections are negligible and the reflected light intensity may be regarded as the results of the interference of two first order reflected beams. The average power level of the probe reaching PD is on the order of 50 μW. By tuning the wavelength of probe to the quadrature point (Q-point) of the FPI, the diaphragm deflection due to PA pressure wave, is linearly and most efficiently converted into light intensity variation at the FPI output [11].

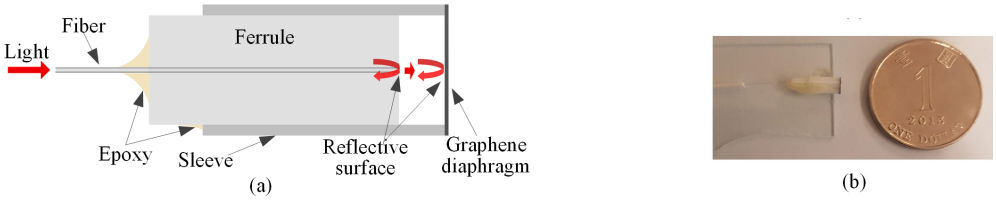

Fig. 2 (a) Schematic diagram of the fiber-tip FPI acoustic detector. (b) Photograph of the fiber-tip FPI acoustic detector.

In most of the reported PA gas cells that use a longitudinal resonant tube for acoustic signal enhancement, the frequency of first acoustic resonance of the resonant tube is at low kHz range, whereas the resonant frequency of our graphene nano-mechanical resonator is around 50 kHz. To match the resonance of the tube to that of the graphene resonator, we designed a micro acoustic resonator (AR) that has a higher resonant frequency. The AR is made by a tube with a hole in the middle and the schematic is shown in Fig. 3. The outer radius of the AR is 3.2 mm, which is the same as with the ceramic sleeve. Small inner diameter of the AR can achieve a larger PA signal but too small size may lead in background noise due to wall absorption [14]. We here selected the inner diameter (*ID*) of tube to be 1 mm, which is more than three times the diameter of the pump beam. To reduce the viscous losses occurring at the hole, the tube was side polished down with a depth of 0.8 mm. The radius of the hole was 0.2 mm. The relationship between the length of the AR tube (l_{AR}) and resonant frequency (f_0) may be expressed as [15]:

$$l_{AR} = \frac{v}{f_0} - \frac{v}{\pi f_0}\arctan\left(\frac{4\pi(ID/2)^2}{r_0^2/(t_0+1.2r_0)}\cdot\frac{f_0}{v}\right) - 0.6ID \qquad (1)$$

where v is the acoustic velocity within the tube, t_0 is the wall thickness of tube and r_0 is the radius of the side hole in the middle of the AR. To match the resonant frequency of the tube to the graphene detector, i.e., f_0= 50 kHz, the optimum length of the AR was calculated to be 4.3 mm.

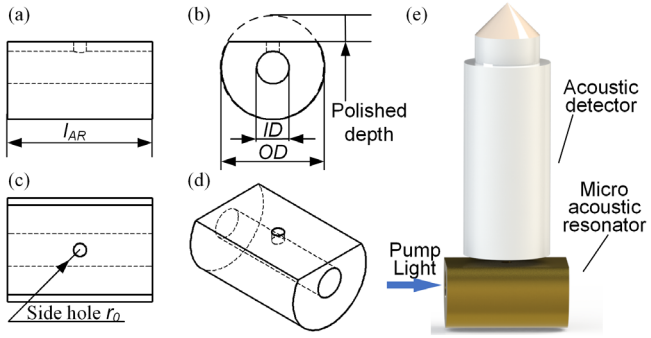

Fig. 3 Schematic diagram of micro AR. (a) Front view. (b) Left view. (c) Top view. (d) Isometric view. (e) 3D rendering of AR and acoustic detector.

III. GAS DETECTION EXPERIMENT

To characterize the PA signal enhancement, we conducted experiment with 100 ppm C_2H_2 balanced by nitrogen (N_2). The wavelength of the ECDL was tuned to 1585 nm corresponding to a Q-point of the FPI acoustic detector. The pump power was fixed to 55 mW and the modulation frequency of pump was varied from 23 to 28 kHz with steps of 200 Hz, corresponding to the 2*f*-frequency from 46 to 56 kHz. The modulation index of the pump laser (defined as the ratio of modulation amplitude to the half width at half maximum of the absorption line) was set to 2.2, where 2*f*-signal at the absorption line center has its maximum value [16]. The time constant of the LIA was set to 1 s, with an 18 dB/octave slope filter, corresponding to an equivalent noise band width of 0.094 Hz.

Fig. 4 shows the 2*f* output signal as a function of pump modulation frequency when the wavelength of the pump laser is fixed to the center of the P(13) line of C_2H_2. The data points in black were obtained without using the AR, which is the characteristic of the graphene resonator. By fitting these data points to a Lorentzian function, the Q-factor of the graphene resonator was determined to be 12 and the optimum modulation frequency for the graphene resonator is ~25 kHz. The data points in red were obtained with the AR. The 2*f* output reaches maximum when the modulation frequency is ~24.4 kHz. The corresponding 2*f* frequency is ~48.8 kHz, which deviates slightly from the designed value of 50 kHz. This frequency dependence is affected by the AR as well as graphene resonator. Both the graphene resonator and AR have resonant characteristics, but the resonant frequencies of the two did not match perfectly, resulting an asymmetric frequency response curve.

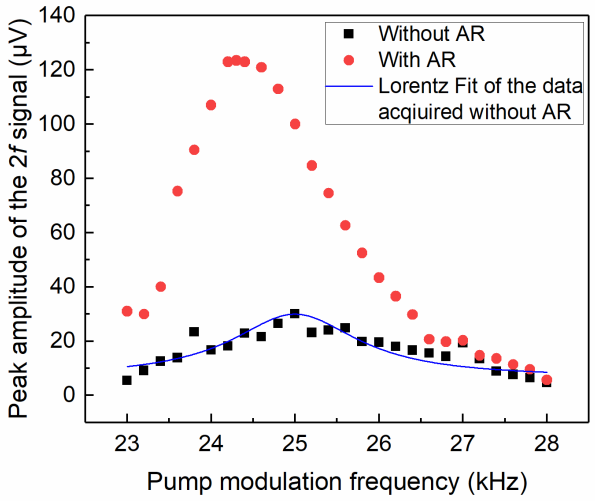

Fig. 4 2*f* lock-in output under different modulation frequencies when the central wavelength of pump laser is fixed to 1532.83 nm. Black squares: Experimental data obtained without using AR. Blue line: Lorentz fitting of the Data without AR. Red dots: Experimental data obtained with AR.

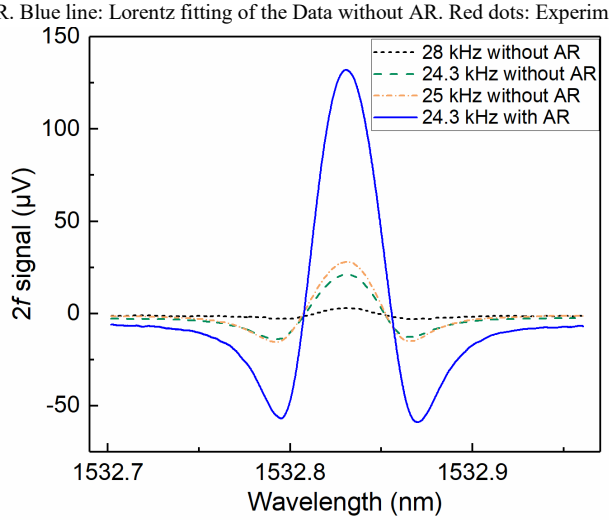

Fig. 5 2*f* lock-in output when the pump wavelength is swept across the P(13) line of acetylene at 1532.83 nm. Black short dash line, acquired at modulation frequency of 28 kHz (off the resonant frequency of graphene membrane) and without the use of AR. Green dash line, acquired at 24.3 kHz and without AR. Yellow dash dot line: acquired at 25 kHz (on the resonant frequency of graphene membrane) and without AR. Blue solid line, acquired at 24.3 kHz and with AR.

The optimum modulation frequency of the pump with the double-resonance enhancement configuration is found to be 24.3 kHz and the 2*f* signals at different frequencies around this value are shown in Fig. 5. For comparison, the results obtained without the AR are also presented. The 2*f* signal amplitude has a significant improvement when the AR is used. The signal amplitude and noise level with/without the AR are listed in Table I. The noise data were obtained by measuring the LIA output when pump wavelength was tuned away from gas absorption line. The time duration for calculating standard deviation (s.d.) of noise is 100 s. The noise

level with the AR is a little lower than that without the AR. We believe it is due to graphene absorption [17] of the scattered pump power, since the graphene diaphragm is placed close to the pump beam when the AR is not used. At 24.3 kHz, the signal-to-noise ratio (SNR) with AR is 6.0 times higher than that only using graphene resonator. Even compared with the value at 25 kHz, the signal still has a 4.9-time improvement.

TABLE I
PERFORMANCE OF GAS SENSOR WITH DIFFERENT TEST CONDITION

Modulation frequency (kHz)	Micro AR	Signal	Noise (1σ μV)	SNR
24.3 (On AR resonance)	With	132.1	0.094	1405.3
24.3	without	21.3	0.105	202.9
25.1 (On graphene resonance)	Without	28.1	0.106	265.1
28.0 (Off graphene resonance)	Without	2.8	0.98	2.9

Fig. 6 shows the 2*f* signal for 100 ppm C_2H_2 balanced by N_2 and noise level as functions of the pump power level. The 2*f* signals for different pump power levels are shown in blue dots. A linear relationship is obtained in the power range of 27 to 138 mW. The s.d. of the noise levels for different pump power levels are shown as black squares. The noise level changed very little when pump power was varied.

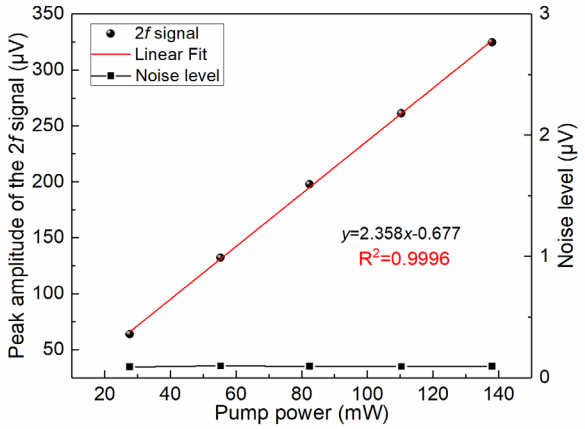

Fig. 6. 2*f* signal and the noise level as functions of the pump power level. The time constant of lock-in is 1 s with a filter slope of 18 dB/octave.

We also measured the 2*f* signal for different gas concentration from 1 to 100 ppm. For these experiments, the probe power is a slightly lower than that for Figs.4-6. Fig. 7(a) shows the 2*f* signals for different C_2H_2 concentration levels when the wavelength of the pump power is tuned across the P(13) absorption line of C_2H_2. The inset in Fig. 7(a) provides the details of the 2*f* signal measured with 1 ppm C_2H_2 and pure N_2 (noise). The peak amplitude of the 2*f* signal is ~2.87 μV. The s.d. of the noise over the range from 1532.7 to 1532.98 nm is 0.071 μV, corresponding to a SNR of 41 [18]. This gives a 1σ noise equivalent concentration (NEC) of 24.7 ppb, corresponding to a normalized noise equivalent absorption (NNEA) of 1.29×10^{-8} $cm^{-1}WHz^{-1/2}$. The 2*f* signals obtained with different concentration levels of C_2H_2 are shown in Fig. 7(b) with black squares. Curve fitting shows a linear relationship between the signal and the gas concentration.

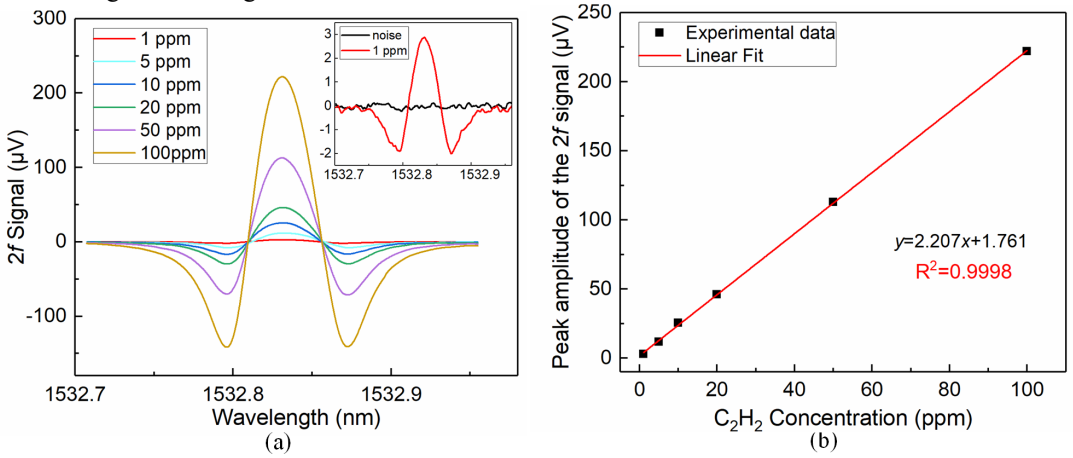

Fig. 7. (a) 2*f* signal spectra with different C_2H_2 concentration levels. Inset: the 2*f* signal measured with 1 ppm C_2H_2 and with pure N_2. (b) 2*f* signal as a function of pump power level. Black dots: experimental data. Red line: linear fit. The time constant of the lock-in is 1 s with a filter slope of 18 dB/octave.

IV. Conclusion

We have demonstrated a PA gas sensor based on double-resonant signal enhancement detection. The sensor is compact in size and comprises a 4.3-mm-long and 3.2-mm-diameter micro AR tube and a 2.5-mm-diamater graphene nano-mechanical resonator. By operating at a frequency matched to the resonances of the AR and the graphene resonator, ~5-fold enhancement of SNR over that with only a graphene resonator is achieved. With a pump power of 138 mW, we obtained a 1σ NEC of 24.7 ppb acetylene, corresponding to a NNEA of 1.29×10^{-8} $cm^{-1}WHz^{-1/2}$.

References

[1] M. Fehér, Y. Jiang, J. P. Maier, and A. Miklós, "Optoacoustic trace-gas monitoring with near-infrared diode lasers," *Applied optics,* vol. 33, no. 9, pp. 1655-1658, 1994.

[2] A. Kosterev *et al.*, "Application of quantum cascade lasers to trace gas analysis," *Applied Physics B,* vol. 90, no. 2, pp. 165-176, 2008.

[3] A. Kosterev, Y. A. Bakhirkin, R. Curl, and F. Tittel, "Quartz-enhanced photoacoustic spectroscopy," *Optics Letters,* vol. 27, no. 21, pp. 1902-1904, 2002.

[4] H. Zheng *et al.*, "Scattered light modulation cancellation method for sub-ppb-level NO 2 detection in a LD-excited QEPAS system," *Optics express,* vol. 24, no. 10, pp. A752-A761, 2016.

[5] K. Wilcken and J. Kauppinen, "Optimization of a Microphone for Photoacoustic Spectroscopy," *Applied Spectroscopy,* vol. 57, no. 9, pp. 1087-1092, 2003/09/01 2003.

[6] V. Koskinen, J. Fonsen, K. Roth, and J. Kauppinen, "Cantilever Enhanced Photoacoustic Detection Of Carbon Dioxide Using A Tunable Diode Laser Source," *Applied Physics B,* vol. 86, no. 3, pp. 451-454, 2007.

[7] J. Ma, W. Jin, H. L. Ho, and J. Y. Dai, "High-sensitivity fiber-tip pressure sensor with graphene diaphragm," *Optics letters,* vol. 37, no. 13, pp. 2493-2495, 2012.

[8] C. Li, X. Gao, T. Guo, J. Xiao, S. Fan, and W. Jin, "Analyzing the applicability of miniature ultra-high sensitivity Fabry–Perot acoustic sensor using a nanothick graphene diaphragm," *Measurement science and technology,* vol. 26, no. 8, p. 085101, 2015.

[9] Q. Wang, J. Wang, L. Li, and Q. Yu, "An all-optical photoacoustic spectrometer for trace gas detection," *Sensors and Actuators B: Chemical,* vol. 153, no. 1, pp. 214-218, 3/31/ 2011.

[10] Y. Cao, W. Jin, H. L. Ho, and J. Ma, "Miniature fiber-tip photoacoustic spectrometer for trace gas detection," *Optics letters,* vol. 38, no. 4, pp. 434-436, 2013.

[11] B. Yu, D. W. Kim, J. Deng, H. Xiao, and A. Wang, "Fiber Fabry-Perot sensors for detection of partial discharges in power transformers," *Applied optics,* vol. 42, no. 16, pp. 3241-3250, 2003.

[12] Y. Tan, C. Zhang, W. Jin, F. Yang, H. L. Ho, and J. Ma, "Optical fiber photoacoustic gas sensor with graphene nano-mechanical resonator as the acoustic detector," *IEEE Journal of Selected Topics in Quantum Electronics,* vol. 23, no. 2, pp. 1-11, 2017.

[13] J. Ma, Y. Yu, and W. Jin, "Demodulation of diaphragm based acoustic sensor using Sagnac interferometer with stable phase bias," *Optics express,* vol. 23, no. 22, pp. 29268-29278, 2015.

[14] F. Bijnen, J. Reuss, and F. Harren, "Geometrical optimization of a longitudinal resonant photoacoustic cell for sensitive and fast trace gas detection," *Review of Scientific Instruments,* vol. 67, no. 8, pp. 2914-2923, 1996.

[15] H. Yi, K. Liu, S. Sun, W. Zhang, and X. Gao, "Theoretical analysis of off beam quartz-enhanced photoacoustic spectroscopy sensor," *Optics Communications,* vol. 285, no. 24, pp. 5306-5312, 2012.

[16] J. Reid and D. Labrie, "Second-harmonic detection with tunable diode lasers — Comparison of experiment and theory," (in English), *Applied Physics B,* vol. 26, no. 3, pp. 203-210, 1981/11/01 1981.

[17] F. Xia, T. Mueller, Y.-m. Lin, A. Valdes-Garcia, and P. Avouris, "Ultrafast graphene photodetector," *Nature nanotechnology,* vol. 4, no. 12, pp. 839-843, 2009.

[18] V. Spagnolo, P. Patimisco, S. Borri, G. Scamarcio, B. E. Bernacki, and J. Kriesel, "Part-per-trillion level SF6 detection using a quartz enhanced photoacoustic spectroscopy-based sensor with single-mode fiber-coupled quantum cascade laser excitation," *Optics Letters,* vol. 37, no. 21, pp. 4461-4463, 2012/11/01 2012.